The effect of Porosity on Tortuosity

Nuradeen Labaran Tanko

Abstract— In recent decades, Tortuosity has been stated to depned on geometric properties of porou media such as the Pore Size Distribution, Pore Size, Pore shape, and many more. However, there is no work in the literature to show a clear relationship between topological properties such as the Tortuosity and Porosity. In this work, a simple geometry correlation for Tortusity of flow path and porosity in porous media is presented. The materials studied are chemically pure mesoporous silica and alumina catalyst support pellets with simplified pore sizes, pore side dsitribution, and surface Chemistry. The Tortuosity of the sample is deduced from PGSE NMR log attenuation plots and the porosity from retraction curves of mercury porosimetry. In closure, a statistically significant correlation exits, and thus verifies the simulation work in the literature where tortusity is shown to decares with an increase in porosity.

Index Terms - Mercury Porosimetry, Mercury Entrapment, Permeabilty, Pore Size Distribution, Porosity, Pulsed Field Gradient Sequence EChoe NMR, Tortuosity

1 Introduction

Oil reservoirs are physically heterogeneous, with layers of different permeabilities. Therefore, oil reservoirs can contain a network of high permeability fractures surrounded by matrix blocks of low permeability. These heterogeneity can be within and between layers. Effective dispersivity and effective permeability are primarily due to heterogeneity between layers. The permeability of a medium is related to the porosity, but also to the shapes of the pores in the medium and their level of connectedness. The size, shape, and arrangement of conducting spaces in porous materials, such as reservoir rocks, are known to affect the flow of fluids and the displacement of one fluid by another [1,2]. Pores and throats of different sizes may be distributed randomly in a network (randomly heterogeneous) or they may be distributed non-randomly [3]. In the latter case, the larger elements may be clustered together in domains and likewise the smaller elements are clustered together in other domains.

In recent years, [4] compared low-porosity carbonate rocks MicroCT images before and after Mercury intrusion. It was found that ink-bottle shape pores and tortuous complex porous systems prevent Mercury from flowing out of the sample at the end of Mercury porosimetry test. On the other hand, low tortuous cylindrical pores allow Mercury flowing out. In a similar approach, [5] investigated the effect of Tortuosity on capillary imbibition in wetting porous media. The researchers obtained the average height growth of wetting liquid in porous media driven by capillary force. A linear relationship turns out to be the case when dealing with straight capillary tube. [6] expanded [5] work on Tortuosity by investigating by coupling the circle and square models. The researchers established a relationship between tortuosity and porosity with different configurations by using a statistical method. In addition, the tortuosity fractal dimension is expressed as a function of porosity. It was found that tortuosity decreases with an increase in porosity in both cases. Therefore, the predicted correlations of the tortuosity and the porosity agree well with the existing experimental and simulated results which was in good agreement with the work of [7-10].

The aforementioned simulation results offer good explanations of the linear correlation between tortuosity and porosity. However, they all share similar limitations, where they failed to verify their findings by conducting experiments on porous media. It is in this regard that this paper further elucidates and expands the work of those researchers on a range of alumina and silica materials. The heterogeneity will be examined with the aid of PGSE NMR. Therefore, the effects from restricted diffusion, and or various domains having different diffusivities, will be investigated. By examining the diffusion behaviour of water within a porous medium, it may be possible to see the changes in tortuosity effects as a function of diffusion time and porosity. In recent decades, the effects from restricted diffusion, and or various domains having different diffusivities in porous media can be studied by the use of Pulsed Gradient Spin Echoe (PGSE) Nuclear Magnetic Resonance (NMR). By examining the diffusion behaviour of water within a porous medium, it may be possible to see the changes in tortuosity effects as a function of diffusion time. However, in the case of slow exchange between two diffusion domains, [11] observed multi-exponential echo decay as each domain would possess its own diffusion coefficient. PGSE NMR has also been applied to porous media in an attempt to obtain both transport and structural information [12]. However, due to Brownian motion, the mean square displacement of molecules is linearly proportional to time in bulk liquids. The proportionality constant is the bulk diffusion coefficient. Therefore, when a fluid is confined in a porous medium, diffusion is restricted by the solid surfaces bounding the void space, so the apparent diffusion becomes a function of observation time [13]. According to [14], at short observation time, the diffusion coefficient is determined by the surface to volume ratio of the pore space. Whilst at longer observation time, diffusing molecules probe the connectivity of the probe space, and thus, the diffusion coefficient is determined. Mercury porosimetry is probably still the only method by which a macroscopic porous material can be characterised using just a single technique. In principle, mercury porosimetry can be used to obtain the porosity, specific pore volume, pore connectivity [15], and the spatial distribution of pore size [16,17]. Despite the limitations addressed above, mercury porosimetry is widely used in characterisation of catalyst support pellets [18,19]; cement based materials [20,21], granite and saprolite materials [22,23], and sedimentary rocks [1,2]. Therefore, this study will adopt mercury porosimetry for the evaluation of porosity.

2 Theory

The study of diffusion by Nuclear Magnetic Resonance (NMR) began back in the early 1950s with the works of [24,25]. Further developments included the use of spin echoes, [26] and stimulated spin echo [27] sequences for studying diffusion coefficients. Most subsequent diffusion sequences are derived from these two sequences [28]. In recent years, the PGSE NRM has been a well-established method for measuring diffusion coefficients in systems ranging from catalyst supports [11,29,30] porous glasses [31,32] to sedimentary rocks [33,14]. Therefore, the PGSE NMR technique have proven to be powerful and popular tools for diffusion studies in porous media. However, there are a number of challenges that might arise if the investigation is to refer to media of a more complex nature such as the

heterogeneous, micro-textured, porous, granular, composite or high-viscosity materials. Consequently, there will be tendencies to anomalous diffusion, superimposed components, extremely small displacement rates, and displacement restrictions [34]. In PGSE NMR, the echo attenuation $(R^{\cdot})$ is defined as the ratio of the echo intensity in the presence of the gradient (I) to the echo intensity obtained in the absence of a gradient (I_0). For unrestricted self-diffusion, where the random motion of the molecules is assumed to follow Gaussian behaviour, the echo intensity (I) is given by [26]:

$$I = I_0 e^{-D\gamma^2 g^2 \delta^2 \left(\Delta - \frac{\delta}{3}\right)} \quad (1.0)$$

where D is the diffusion coefficient, γ is called gyromagnetic ratio of the observed nucleus, g is the gradient strength, δ is length of the gradient pulse, and Δ is the diffusion time. A range of echo attenuations are obtained by varying g, δ or Δ. Equation 1.0 can be used to calculate diffusion coefficient of the observed nucleus in a homogeneous system. Therefore, in the case of isotropic bulk diffusion, a plot of $\ln\left[\frac{I}{I_0}\right]$ against the group $\xi = \left[\gamma^2 g^2 \delta^2 \left(\Delta - \frac{\delta}{3}\right)\right]$ yields the diffusion coefficient from the slope of the straight line obtained [11]. The diffusion coefficient is obtained by labelling the position of the molecules at the start of the experiment through the use of a field gradient. After a certain period of time (diffusion time, Δ), during which the molecules will have moved to a different random position due to self-diffusion, the positions of the molecules are labelled again by a second gradient [35]. The final signal observed will be a function of the diffusion coefficient D_0, the gradient strength g, δ, and the diffusion time Δ [35]. A typical pulse sequence is illustrated in Figure 1.0

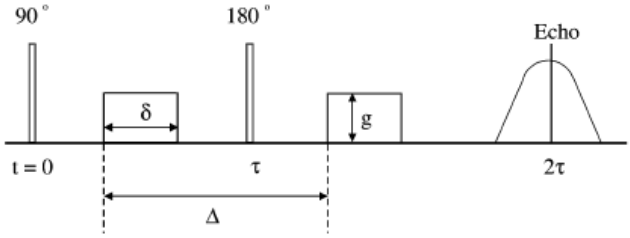

Figure 1.0
A schematic diagram of the pulse sequence that was first introduced by [26]

In general, a linear log-attenuation plot suggests diffusion of a single component in a homogeneous environment and Equation 1.0 describes the relationship between signal attenuation and the diffusion coefficient. The effective diffusion coefficient calculated from a one component fit will be characteristic of the average motion of all molecules and, therefore, will be a combination of free diffusion and restricted diffusion. With a very small value of a short diffusion time (Δ) none of the molecules will be restricted as none of the molecules will have sufficient time to reach the walls of the pores. Therefore, the effective diffusion coefficient measured is that of molecule in free solution. In contrast, if the diffusion time (Δ) is sufficiently large all the molecules contained within the pores will contact the pore walls and thus undergo restricted diffusion. Consequently, non-linearity in the echo-attenuation plot will be observed if the molecules sample regions associated with largely varying diffusion coefficients. Hence, the long-time behaviour of diffusion coefficient provides an indirect measure of the macroscopic structure [35]. A discrete multicomponent model was derived by [11], Equation 2.0, where the heterogeneity in the apparent diffusion coefficient is attributed to i components, each containing the fraction, p_i, of observed nuclei, with the actual diffusion coefficient, D_i, where ξ is characteristic of the experimental parameters $\left[\gamma^2 g^2 \delta^2 \left(\Delta - \frac{\delta}{3}\right)\right]$.

$$I = I_0 \Sigma p_i \exp(-D_i \xi) \quad (2.0)$$

In a PGSE NMR experiment, the diffusion time can be varied from a few milliseconds up to several seconds. Because of effects from the restricting geometry, the measured self-diffusion coefficient (D) depends on the diffusion time (Δ). The measured self-diffusion (D) is also sensitive to physical parameters like permeability and the volume fraction of the diffusing species. The measured self-diffusion (D) can be related to certain characteristics of the porous medium such as the surface-to-volume ratio and the tortuosity (τ). The measured self-diffusion (D) of a diffusing fluid is found to decrease with observation time (Δ) and reaches a plateau value. That plateau value represents the tortuosity (τ) of the system [36]. The effective self-diffusion coefficient (D_{eff}) is a measure of how the water is diffusing within the porous network. Therefore, the tortuosity of a pore network (τ) is a measure of the potential deviation from a linear path that a diffusing molecule may experience. For the diffusion of a liquid in a porous solid, the effective diffusivity of the liquid in the material is related to the molecular self-diffusion coefficient (D_0) of the bulk liquid as follows [11]:

$$D_{eff} = \frac{D_0 \varepsilon}{\tau}, \quad (3.0)$$

where ε voidage of the material. The voidage term is traditionally ignored since the observed signal contains spin density which is directly proportional to voidage. Therefore, Equation (3.0) can be written as:

$$D_{eff} = \frac{D_0}{\tau}, \quad (4.0)$$

where D_0 is the diffusion coefficient of the bulk liquid. Traditionally water is used as the bulk liquid. In general, tortuosity (τ) describes the geometry of flow paths, thus, a measure of the complexity of a porous medium. It is as a conceptual, dimensionless number representing the departure of a porous system from being composed of straight pores. Since fluid travels along a tortuous path through the medium, the actual or effective pore length (l_{eff}) is greater than the average linear flow path length (l_p). The ratio of the two lengths defines tortuosity [37]. In porous media, tortuosity depends on how well the pores are connected [14].

$$\frac{\text{Effective flow path}}{\text{Average linear flow path}} = \frac{l_{eff}}{l_p} = \tau \qquad (5.0)$$

Furthermore, the total tortuosity (τ) of a porous solid can be considered to have independent contributions from tortuosity on various length scales. The total tortuosity can considered as the product of these independent tortuosities since the effective diffusivity will decrease monotonically with scale [12]. Therefore, the PGSE (NMR) experiment measures:

$$\tau = \tau_e \tau_\mu ,$$

(6.0)

where τ_e is the mesoscopic contribution to the tortuosity over length scales of a few pore diameters up to scales at which macroscopic heterogeneities become significant, and τ_μ characterizes tortuosity over length scales of up to a few pore diameters [12]. However, if the molecules diffuse between compact particles, the effective restricted interparticle diffusion coefficient is [14,35],

$$\frac{D_{eff}}{D_0} = \frac{D_{\text{int}er}}{D_0} = \frac{\varepsilon_b}{\tau} ,$$

(7.0)

where ε_b is the particle bed porosity and τ the tortuosity that the molecules experience diffusion through the bed of particles. The particular storage capacity of a porous media is called porosity. It is usually is defined as a ratio of the pore volume (void space) in a catalyst to the total volume (bulk volume) and it is expressed as a percentage. The void space is the summation or combined volume of all the pore spaces in a given porous material. It is donated by ϕ or ε and expressed by the following relationship:

Porosity = Pore volume/Total or bulk volume (8.0)

The effective porosity value is the quantitative value desired and it's used in almost all calculations because it represents the pore occupied by mobile fluids. The porosity can be obtained with the aid of mercury porosimetry. PGSE NMR is limited by the time scale used for probing samples, and thus not the most suitable method of porosity evaluation. Gas adsorption and mercury porosimetry are complementary methods with the latter covering a much wider size range (0.0035 to 500 μm). Mercury porosimetry can give information that is valuable in assessing multiphase fluid behaviour of oil and gas in a strongly water-wetting system and the trapping of oil or gas that is controlled mostly by capillary forces, and thus, a direct analogy with the air-mercury system is possible [38]. It is in this regard that this study adopts Mercury porosimetry for the samples under investigation. In mercury porosimetry, the Laplace equation, also known as the Washburn equation, can be employed to relate an applied pressure with a relevant pore diameter being intruded by the non-wetting liquid mercury.

$$\Delta p = \gamma_{HG}\left(\frac{1}{r_1} + \frac{1}{r_2}\right) = \frac{2\gamma_{HG}\cos\theta}{r_P} \qquad (9.0)$$

The Washburn equation (Equation 9.0) relates the pressure difference across the curved mercury interface (r_1 and r_2 being the radii of curvature of that interface) to the corresponding pore size (r_p) using the surface tension of mercury (γ_{HG}) and the contact angle (θ) between the solid and mercury. The volume of mercury penetrating the pores is measured directly as a function of the applied pressure. According to [39], a value of 0.485 N/m at 25 ˚C is generally accepted for surface tension and a fixed value of 130° for the contact angle (irrespective of the sample material). However, the surface or interfacial tension of mercury contributes greatly with respect to errors in the determination of the pore size distribution and can change with pore size [39]. The total pore volume is the total volume of intruded mercury at the highest pressure.

2.3 Materials

The materials studied in this work are commercially available, chemically pure mesoporous silica and alumina catalyst support pellets with simplified pore sizes, pore size distribution, and surface chemistry. As highlighted in Table 1, the materials have pore size lying in the range of 7-30 nm. The majority of the materials have unimodal structure with the exception of one bimodal structured material (AL3984T).

Table 1.0
A range of alumina and Silica materials tested

S/N	Sample	Material	Pellet form	Voidage	Nominal diameter (mm)
1	Aerosil	Silica (SiO_2)	Fumed sphere	N/D[a*]	3.5
2	AL3984T	Alumina (Al_2O_3)	Tablet	0.59	3.0
3	AL3992E	Alumina (Al_2O_3)	Extrudate	0.65	3.0
4	C10	Silica (SiO_2)	Gel sphere	0.66	3.0
5	C30	Silica (SiO_2)	Gel sphere	0.69	3.0
6	P7129	Silica (SiO_2)	Gel sphere	0.67	3.0
7	Q17/6	Silica (SiO_2)	Gel sphere	0.49	3.5
8	S980A	Silica (SiO_2)	Gel sphere	0.6	3.0
9	S980G	Silica (SiO_2)	Gel sphere	0.61	2.2

10	Silica Alumina	Silica and Alumina (Al_2O_5Si)	Extrudate	0.60	0.5

Note: a* – Not detected

2.4 Experimental Consideration

2.4.1 PGSE NMR

The samples were prepared by impregnation with deionised water, under ambient conditions, in a beaker for at least 24 hours. However, before any impregnation, the big pellets, such as Aerosil and Q17/6 tablets, were sliced into appropriate sizes that could readily fit into an NMR sample tube. It was essential to allow the liquid to fully imbibe the porous network. However, excess water was removed from the pellet's external surface by contacting each pellet with pre-soaked tissue paper as demonstrated by [40]. Also, PGSE NMR phenomena are sensitive to the chemical and physical environments of a molecule such as temperature in particular [11]. Therefore, the diffusion coefficient of bulk liquid (deionized water) was measured before and after each sample analysis. This was necessary in order to detect any slight temperature difference. A quartz tube filled with deionised water to a height of around 5 cm was used for estimating the diffusion coefficient, D_0, of the bulk liquid. All PGSE NMR experiments were performed by using a Bruker AV400 NMR spectrometer, with a broadband (BBO) multinuclear probe equipped with $z-$ gradient coils. The magnet has static field strength of 9.4 T, yielding a proton resonant frequency of 400.13 MHz for ^1H nucleus. The gradients were supplied by a Bruker Grasp II unit, and the maximum attainable gradient strength was 53.5 G cm^{-1}. The maximum sample length was constrained by the region over which uniform linear gradients could be produced and is 15 ± 1 mm. It was assumed that the magnetic field was uniform and there was no cross-relaxation with the sample. All experiments were conducted at temperatures of 25 ± 0.5 °C. The acquisition parameters used are given in Table 2.0. The data acquisition was controlled by a computer. For the bulk liquid diffusion analysis, acqusition Set 1 was used; where as in the case of sample diffusion analysis, both acquision Sets 1 and 2 were used. A series of eight spectra were taken at increasing gradient strengths and the number of scans for each spectrum was 16. Signal attenuation was used to calculate the diffusion coefficient and comparative tortuosities of the water confined within the samples.

Table 2.0
Experimental acquisition parameters used for PGSE NMR technique

Parameter	Acquisition set	
_	1	2
Gradient strenght, g (G cm^{-1})	0.674 to 32.030	0.674 to 32.030
Diffusion time, Δ (s)	0.05	0.1
Gyromagnetic ratio, γ ($radT^{-1}s^{-1}$)	2.765	2.765
Duration of the gradient, δ (s)	0.02	0.02
Bi polar correction delay, τ_T (s)	0.0001	0.0001

- *Author name is currently pursuing masters degree program in electric power engineering in University, Country, PH-01123456789. E-mail: author_name@mail.com*
- *Co-Author name is currently pursuing masters degree program in electric power engineering in University, Country, PH-01123456789. E-mail: author_name@mail.com*

(*This information is optional; change it according to your need.*)

2.4.2 MERCURY POROSIMETRY

The AutoPore III 9420 mercury porosimeter is designed to perform low pressure analysis of four samples at one time. The equipment is designed to perform two high pressure analyses at the same time. The equipment measures the intruded volume in relation to the mass of the sample at a specific pressure; this pressure can be converted to an equivalent Laplace diameter according to Washburn Equation $\left[\Delta P = \frac{2\gamma_{HG}\cos\theta}{r_p}\right]$. The amount of mercury intruded is determined by the fall in the level of the interface between the mercury and the compressing fluid. A value of 0.485 Nm^{-1} at 25 °C is generally accepted for surface tension and a fixed value of 130° for the contact angle, as a result, were adopted in this study. If less than four samples are to be analysed, a blank rod must be installed in the unused low pressure ports. Vacuum conditions cannot not be achieved if penetrometers or blank rods are not installed in an unused pressure port.

Porous materials are prone to adsorb water or other chemicals, and therefore the sample has to be cleared of these contaminants before the analysis by heating. The purpose of the thermal pretreatment for each sample was to drive any physisorbed water on the sample leaving the morphology of the sample itself unchanged. A pretreatment condition of 250 °C for 4 hours used by [41] was adopted for this study. A powder penetrometer (3cc powder) was used due to the small physical size of the materials. The weight of the empty sample flask was registered prior to introducing the sample. The sample (~ 0.7 g) was loaded into the penetrometer, which consisted of a sample cup connected to a metal-clad, precision-bore, and glass capillary stem. A vacuum tight seal (Apiezon H) was used to fill the inevitable roughness of the ground glass lip and polished surface. Care was taken when applying the grease as too much grease exposes the sample to an unwanted coating, whilst too little grease results in an imperfect seal. The penetrometers were sealed with spacers over the stem and placed in low pressure ports, where the sample was evacuated to remove air and moisture. The sample cell was evacuated and filled with mercury while the entire system was still under reduced pressure. The first data point was taken at a pressure of 3000 to 4000 Pa or higher. At the end of the low pressure analysis, the weight of the penetrometer filled with mercury and sample was determined. The measured value determines the bulk density of the sample by using corresponding blank-runs as a reference. Once the preweighed sample from the low pressure analyses port was transferred to the high pressure system, the sample and the injected mercury from the low pressure system was surrounded by hydraulic fluid and pressurised up to 414 MPa. Both chambers were tightly closed and had sufficient high pressure fluid drawn into the vent valve. If the fluid was above the visible ledge level, excess fresh fluid was removed to bring the level to the ledge. In order to calculate the true volume intrusion of mercury into the pores of a sample, a correction was made to account for the compression of mercury, sample cell and sample. Compressibility (β^0) is the fractional change in volume per unit pressure change and therefore a major effect that has to be addressed [42]. Ideally, this problem can be corrected by a corresponding blank run using a non-porous sample of the same material. However, the blank run does not always solve the problem as encountered in the course of these experiments. One of the adjustments made was to create separate blank runs with the same respective equilibration time as those used in the experiments.

4 RESULT AND ANALYSIS

Repeat measurements were made on the bulk probing liquid sample (deionised water) on the same day at constant temperature and yielded diffusion coefficients agreeing to within 0.8 %. For each data set of the probing bulk liquid, the coefficient of determination (R^2) yielded a correlation coefficient greater than 0.999. The self-diffusion coefficient of water at 25 °C was nearly 2.5 ×10^{-9} (± 3.29×10^{-11}) m^2/s in each analysis. The average diffusion coefficient of bulk liquid was considered for calculations. A range of porous alumina and silica pellets of spherical and cylindrical geometry were investigated. A minimum of seven fully saturated pellets were probed in each analysis. The data of the sample was subsequently averaged. Therefore, the sample mean error for the tortuosities and displacements are what are presented in this Section. The reported uncertainties are the 95% confidence intervals that indicate the spread of the results over samples from the same batch and the error associated with the PGSE NMR measurement. These uncertainties indicate the reliability of tortuosity estimates for the diffusion times used in this study. Also, in order to allow for the variation of support structure between pellets from the same batch and to test the reproducibility of measurements, replicate measurements were made for all batches. The apparent tortuosity of the samples were calculated by using the diffusion correlation in Equation 4.0. In the case of suspected deviation from linear behaviour, further replicate measurements (up to two repeats) were made to confirm the true nature of the sample. The number of scans was also doubled. The number of scans was increased to ensure better results and consequently reduce the effect of errors associated with measurement, such as the signal to noise ratio. Also, a two component model was used to fit the curve in some of the plots with concave curve characteristic of a heterogeneous sample. The Microsoft Excel Solver was used to estimate the model parameters such as the intensity, diffusivities and their respective fraction in each domain within the sample. These model parameters from Solver were then used as the first guess in Origin 6.1 software to generate better parameters, along with their respective errors.

Table 3.0
Average key pore geometry characteristics obtained by complimentary methods. The error quoted is the standard error

	Characterization Technique			
	Mercury Porosimetry		PGE NMR	
			Tortuosity	
Sample	Porosity (%)	Pore Diameter (nm)	(Δ = 50 ms) (-)	(Δ = 100 ms) (-)
Aerosil	[1]N/A	[1]N/A	1.59 ± 0.06	1.86 ± 0.09
AL3984T	54.95 ± 2.04	11.85 ± 0.15	1.75 ± 0.03	1.81 ± 0.04
AL3992E	66.10 ± 18.84	9.55 ± 0.05	1.76 ± 0.02	1.85 ± 0.03
C10	67.81 ± 2.16	9.00 ± 0.01	1.57 ± 0.01	1.63 ± 0.04
C30	70.51 ± 3.06	27.90 ± 2.07	1.41 ± 0.01	1.49 ± 0.05
Q17/6	49.06 ± 1.49	6.70 ± 0.10	2.38 ± 0.03	2.42 ± 0.05
S980A	62.55 ± 2.88	11.60 ± 0.30	1.75 ± 0.02	1.81 ± 0.04
S980g	60.25 ± 1.42	38.15 ± 2.15	1.54 ± 0.02	1.57 ± 0.04
Silica Alumina	60.54 ± 2.14	7.45 ± 0.05	2.05 ± 0.04	2.19 ± 0.07

Note: [1]N/A - Not applicable

Furthermore, during the course of Mercury Porosimetry experiments, batch variability was addressed, and thus, in order to allow for the variation of support structure between pellets of the same batch and to test the reproducibility of measurements, replicate measurements were made for all samples. The reported parameters in this section are the mean of these sets used. After each pressure change, the volume of mercury within the sample was then allowed to come to equilibrium over a period of time. The equilibration time at each of the increasing applied pressures of mercury was set at 50 s. The total pore volume estimated in this Section is the total volume of intruded mercury at the highest pressure. The porosity is deduced from Equation 8.0. Please note the equipment automatically give the values after experimentation. Tables 3.0 presents the estimated Porosity, Pore Diameter, and Tortuosity of the investigated materials. Aforementioned, the reported uncertainties indicate the spread of the results over samples from the same batch, and the error associated with the technique. The error bars for measurements obtained at Δ = 50 ms and Δ = 100 ms overlapped for most samples, and thus, there was no significant effect of the diffusion time used on tortuosity in most of the samples. In contrast, Aerosil and C30 (the least tortuous sample is C30) were sensitive to the diffusion time. Therefore, Aerosil and C30 are the only samples where the tortuosity varied with length scale for the range of values studied. Figures 2.0 to 3.0 present the effect of Tortuosity on Porosity at short and long diffusion time, respectively. It can be seen from Figures 2.0 to 3.0 that the Tortuosity decreases with an increase in porosity.

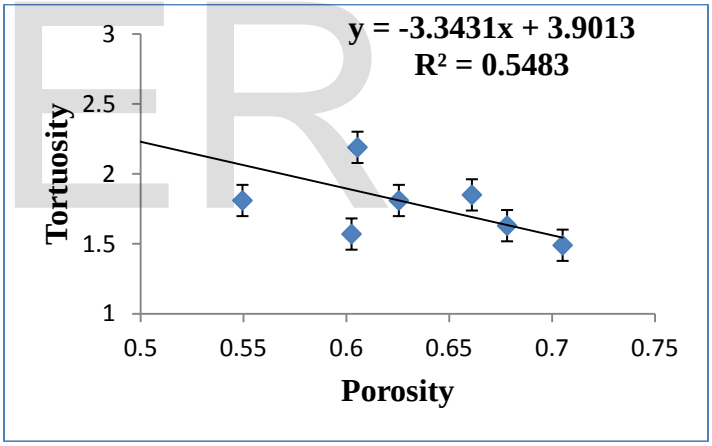

Figure 2.0
Relating ultimate entrapment with tortuosity at short diffusion time

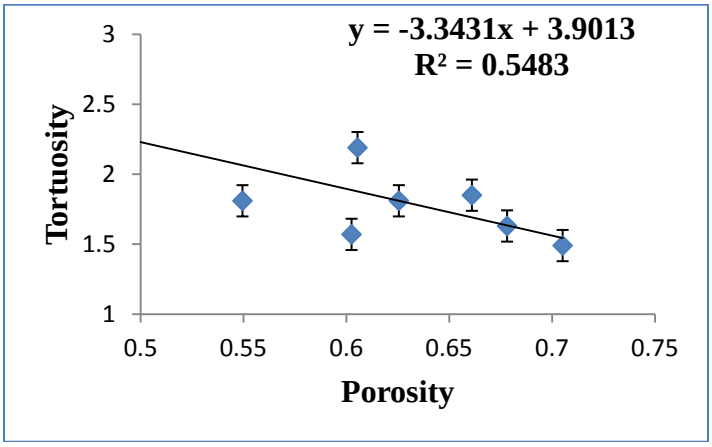

Figure 3.0
Relating ultimate entrapment with tortuosity at long diffusion time

5.0 Discusion

A novel multi-technique approach has been used to derive structural-topological relationships in order to understand the mechanism of ultimate entrapment in porous materials. As detailed in Section 1.0, several researchers used two and three dimensional bond networks simulation to determine the relationships between structural and transport properties in artificial porous materials. Other workers established a relationship between tortuosity and porosity with different configurations by using a statistical by coupling the circle and square models [5]. It was found that tortuosity decreases with an increase in porosity in both cases. Therefore, the predicted correlations of the tortuosity and the porosity agree well with the existing experimental and simulated results of [8,9]. It in this regard that this section discusses these correlations for structural-topological relationships that were tested with experimental results for a range of porous alumina and silica pellets of spherical or cylindrical geometries. During the course of the mercury porosimetry experiment, the pressure was either increased or decreased in small steps, and thus, this might have affected the pore network of the samples. The high hydraulic pressure applied on materials during intrusion can sometimes lead to partial collapse of the pore network or alteration of the sample during the experiments. Therefore, these pressures may also give rise to potential collapse of the unoccupied pores. Consequently, this will reduce the number of large pores and give false entrapment values [43]. This research has been altered to avoid such limitations, such as the mechanical damage of samples. It is noteworthy to mention that all samples were visually observed after the experiments, to ensure that the high hydraulic pressure applied on the materials did not cause elastic or permanent structural changes. The majority of the test samples retained their external structural stability except for C10, AL3992E, and Silica Alumina. Furthermore, the presence of pore shielding in these materials was previously studied by [44]. It was found that no structural deformation or collapse occurred for these samples.

The application of PGSE NMR diffusion measurements is sensitive to the structure of a medium over a scale comparable to the r.m.s displacement of molecules during the experimental time scale of 10^{-3} to 1 s [28]. The PGSE NMR studies of liquid self-diffusion within porous medium give information on the pore structure itself. Therefore, the diffusion measurements of these materials are the absolute estimated values with respect to the probing bulk liquid (deionised water) used. In addition, the effect of structural damage was limited by cutting the big samples (Aerosil and Q17/6) with a small saw. In general, the PGSE NMR method does not probe length scale equivalent to the dimension of the whole pellet. The method is only limited to the length scale of the probe, and thus, the effect of structural damage in those big samples was negligible in the collected data. Therefore, in order to elucidate transport phenomena in porous media, the interconnectivities of the pore system of a wide range of porous alumina and silica pellets were examined by diffusion over two diffusion time-scales (Δ = 50 and Δ = 100 ms). The porosity quoted in Table 3.0 was barely affected by the experimental equilibration time, and thus, was considered as the ultimate porosity. As presented in Table 3.0, the Toruosity of the materials was obtained by using Equation 4.0. The estimated displacements were far greater than the average pore sizes, and thus, this rules out the possibility of restricted diffusion for the length scales studied. In addition, if restricted diffusion was present, then from the Stokes-Einstein relation, Equation 9.0, by the same factor for an increase in diffusion time, there would be a decrease in diffusion coefficient. Furthermore, it can be seen in Figures 2.0 to 3.0 that the amount of Tortuosity decreases with an increase in Porosity. To support this correlation, static analysis was carried out in order to rule out any possibility of random chance. A common alpha level for research is 0.10, and was thus adopted in this study [45]. The number of data points is eight and correlation coefficient obtained was 0.548 and 0.623 at short and long diffusion time respectively. Therefore, by using the critical value table for Pearson's correlation coefficient [45], it can be concluded that the correlation is statistically significant. This significant finding are in good agreement with the simulation works of [7-10].

6.0 Conclusion

A novel multi-technique approach has been used to predict the relationships between Tortuosity and mercury entrapment. A range of porous alumina and silica pellets of spherical or cylindrical geometries were investigated. In this study, a good statistical correlation was obtained. It was proven that Tortuosity decreases with an increase in porosity, despite limitations on the measurement of these descriptors. This finding is in good agreement with several two and three dimensional bond networks simulation work and basic simulation experimental work.

ACKNOWLEDGMENT

The authors thanks Professor S.P. Rigby for his valuable discussion in this research.

REFERENCES

[1] Tsakiroglou, C.D., and Payatakes, A.C. A new simulator of mercury porosimetry for the characterization of porous materials. *Journal of Colloid and Interface Science*, 1990, 137, 315-339.

[2] Tsakiroglou C. D., Payatakes A. C. Mercury Intrusion and Retraction in Model Porous Media, *Adv. Colloid Interf. Sci.*, 1998, 75, 215–253.

[3] Dullien, F.A.L. *In porous media; Fluid transport and pore structure*. 2nd edition. New York: Accademic press. 1992.

[4] Fusi, N., and Martinez, J.M. Mercury porosimetry as a tool for improving quality of micro-CT images in low porosity carbonate rocks. *Engineering Geology*, 2013,166, 272-282.

[5] Cai, J., and Yu, B., 2011. A Discussion of the Effect of Tortuosity on the Capillary Imbibition in Porous Media. *Transport in Porous Media*, 89(2), 251–263.

[6] Jian-Long, K., Xue-Ming,T., Hai-Yan, Z., Hang-Jun, L., Feng-Min, W., You-Sheng, X., and Yong-Sheng, D. Tortuosity for streamlines in porous media. Chin. Phys. B, 2011, Vol. 21, No. 4, 044701.

[7] Matyka, M., Khalili, A., and Koza, Z. Tortuosity-porosity relation in porous media flow. *Physical Review E* 78, 2008, 026306.

[8] Fernie, S., and Latief, F.D.E. Tortuosity–Porosity Relationship in Two-Dimensional Fractal Model of Porous Media. *Fractals*, 2013, 21, 1350013.

[9] Lu, L., Yu, B., Cai, J., Xeng, X. Numerical Simulation of Tortuosity for Fluid Flow in Two-Dimensional Pore Fractal Models of Porous Media. *Fractals* 22, 2014, 1450015.

[10] Duran, L., Hernandez, A., Holek, S. Relation between the porosity and tortuosity of a membrane formed by disconnected irregular pores and the spatial diffusion coefficient of the Fick-Jacobs model. *Physical Review E*, 95, 2010, 052804.

[11] Hollewand, M.P., and Gladden, L.F. Transport heterogeneity in porous pellets-I. PGSE NMR studies. *Chemical Engineering Science*, 1995a, 50, 309-326.

[12] Rigby, S.P., and Gladden, L.F. The use of magnetic resonance images in the simulation of diffusion in porous catalyst support pellets. *Journal of Catalysis*, 1998, 173 (2), 484-489.

[13] Valiullin, R., and Skirda, V.. Time dependent self-diffusion coefficient of molecules in porous media *Journal of chemical physics*, 2001,114 (1), 452-458.

[14] Kleinberg, R.L., Kenyon W.E., and Mitra P.P. Mechanism of NMR relaxation of fluids in rock. *Journal of magnetic resonance series A*, 1994, 108, 206-214.

[15] Portsmouth, R.L., and Gladden, L.F. Mercury porosimetry as a probe of pore connectivity. *Chemical Engineering Research and Design*, 70 (1), 63-70. 1992.

[16] Rigby, S.P. A Hierachical Model for the Interpretation of Mercury Porosimetry and Nitrogen Sorption. *J. Colloid and Interface Sci*., 2000, 224, 382–396.

[17] Rigby, S.P., and Chigada, P.I. Interpretation of integrated gas sorption and mercury porosimetry studies of adsorption in disordered networks using mean-field DFT. *Adsorption-journal of the international adsorption society*, 2009, 15 (1), 31-41.

[18] Rigby S. P., Fletcher R.S., Riley S. N. Determination of the cause of mercury entrapment during porosimetry experiments on sol–gel silica catalyst supports. *Applied Catalysis (A),* 2003b, 247, 27–39.

[19] Ghaly, G. , Beurroies, I., and Ragai, J. Mesoporous Titania Gels Prepared from Titanous Chloride and Ammonia: SEM, Nitrogen Adsorption, Thermoporometry and Mercury Porosimetry Studies. Adsorption Science & Technology, 2010, Vol. 27 No. 10.

[20] Abell, A., Willis, K., Lange, D. Mercury intrusion porosimetry and image analysis of cement-based materials. *J Colloid Interface Sci*, 1999, 211, 39–44.

[21] Ma, H. Mercury intrusion porosimetry in concrete technology: Tips in measurement, pore structure parameter acquisition and application. *J Porous Mater*. 2014, 21:207–215.

[22] Stefan, D., Harald, B., Anna, S., Günter, K., Thomas, R. Determination of Porosity and Pore Connectivity in Fieldspares from Soils of Granite and Saprolite. Soil Science: 2006, 171(9), 675-694.

[23] Turturro, A.C., Caputo, M.C., and Gerke, H.H. Mercury porosimetry for comparing piece-wise hydraulic properties with full range pore characteristics of soil aggregates and porous rocks. *Geophysical Research Abstracts*, Vol. 19, 2017, EGU2017-18729-1.

[24] Hahn, E.L. Spin echoes. *Physical review*, 1950, 80 (4).

[25] Carr, H.Y., and Purcell, E.M., 1954. Effects of Diffusion on Free Precession in Nuclear Magnetic Resonance Experiments. *Phys. Rev*., 94, 1954, 630–638.

[26] Stejskal, E. O., and Tanner J.E. Spin diffusion measurements: spin echoes in the presence of a time dependent field gradient. *Journal of Chemical Physics*, 1965, 42,288 -292.

[27] Tanner, J. E. Use of the stimulated echo in NMR diffusion studies. *J. Chem. Phys*., 1970, 52, 2523–2526.

[28] Callaghan, P. T., 1984. Pulsed field gradient nuclear magnetic resonance as a probe of liquid state molecular organisation. *Aust. J. Phys*., 1984, 37, 359-387.

[29] Rigby, S.P. NMR and modelling studies of structural heterogeneity over several lengthscales in amorphous catalyst supports. *Catalysis Today*, 1999, 53 (2), 207-223.

[30] Farrher, G., Ardelean, I., Kimmich, R. Time-dependent molecular diffusion in partially filled porous glasses with heterogeneous structure. *Applied magnetic resonance*, 2008, 34 (1-2), 85-99.

[31] Pimenov, G.G., and Skirda, V.D. NMR Study of the Kinetics of Butane and Hexane Adsorption from Vapour Phase by Porous Glasses. *Colloid Journal*, 2005, Vol. 67(6), 746–750.

[32] Nechifor, R., Badea, C., and Ardelean, I. Nuclear magnetic resonance studies of liquids morphology inside partially saturated porous media. *Journal of physics: conference series*, 2009,182 (1).

[33] Callaghan, P., Macgowan, D., Packer, K.J., and Zelaya, F.O. Influence of field gradient strength in nmr-studies of diffusion in porous-media. *Magnetic Resonance Imaging*, 1991, 9 (5), 663–671.

[34] Cadar, C., Cotet, C., Baia, L., Barbu-Tudoran, L., Ardelean, I. Probing into the mesoporous structure of carbon xerogels via the low-field NMR relaxometry of water and cyclohexane molecules. *Microporous and Mesoporous Materials*, 2017, 251, 19-25.

[35] Veith, S.R, Hughes, E., Vuataz, G., and Pratsinis, S.E. Restricted diffusion in silica particles measured by pulsed field gradient NMR. *Journal of Colloid and Interface Science*, 2004, 274, 216–228.

[36] Latour, L.L., Kleinberg, R.L., Mitra, P.P., Sotak, C.H. Pore-Size Distributions and Tortuosity in Heterogeneous Porous Media. *Journal of Magnetic Resonance*,1995, Series A, Vol. 112, 83-91.

[37] Scholes, O.N., Clayton, S.A., Hoadley, A.F.A, and Tiu, C. Permeability anisotropy due to consolidation of compressible porous media. *Transport porous media*. 2007, 68 365-387.

[38] Chatzis, I., Morrow, N.R., Lim, H.T. Magnitude and detailed structure of residual oil saturation. *SPE Journal*, 1983, 23, 311–326.

[39] Allen, T. *Particle size measurement*. Dordretch, The Netherlands: Kluwer Academic publishers. 1999.

[40] Hollewand M.P., Gladden L.F. Heterogeneities in structure and diffusion within porous catalyst support pellets observed by NMR Imaging. *Journal of catalyst*, 1993, 144, 254-272.

[41] Evbuomwan, O.E. *The structural characterisation of porous media for use as a model reservoir rocks, adsorbents and catalyst*. Thesis (PhD). University of Bath. 2009.

[42] Giesche H., 2006. Mercury porosimetry: A general (practical) overview. *Particle and particles system characterisation*, 23, 9–19.

[43] Pirard R., Heinrichs B., Pirard J.P. in: McEnaney B., Mays T.J., Rouquerol J., Reinoso R.F., Sing K.S.W., Unger (Eds.) K.K. *Characterisation of Porous Solids IV, Royal Society of Chemistry*,1997, Cambridge.

[44] Rigby S. P., Fletcher R.S., Riley S. N. Determination of the cause of mercury entrapment during porosimetry experiments on sol–gel silica catalyst supports. *Applied Catalysis (A),* 2003b, 247, 27–39.

[45] Chatfield, C. *Statistics for technology: A course in applied statistics*, 1983, Chapman & Hall/CRC.